Research Square

Preprints are preliminary reports that have not undergone peer review.
They should not be considered conclusive, used to inform clinical practice,
or referenced by the media as validated information.

Grid Integrated Analysis of Hybrid Photovoltaic and Wind Power Generation

CHNADRA PRAKASH VERMA (cpv@aith.ac.in)
Dr Ambedkar Institute of Technology
K S Verma
Kamla Nehru Institute of Technology
SATYENDRA SINGH
Institute of Engineering and Technology

Research Article

Keywords: time-domain simulations, dynamic stability, photovoltaic array, linear permanent-magnet generator, root-loci analysis, super-capacitor supply power grid

Posted Date: November 7th, 2022

DOI: https://doi.org/10.21203/rs.3.rs-528495/v1

License: This work is licensed under a Creative Commons Attribution 4.0 International License.
Read Full License

GRID INTEGRATED ANALYSIS OF HYBRID PHOTOVOLTAIC AND WIND POWER GENERATION

CHNADRA PRAKASH VERMA†, K.S.VERMA‡ and SATYENDRA SINGH++

† *Electrical Engineering Department, Dr. Ambedkar Institute of Technology for Handicap Kanpur, India.*
cpv@aith.ac.in
‡ *Electrical Engineering Department, Kamla Nehru Institute of Technology, Sultanpur, India*
ksv211@rediffmail.com
++ *Electrical Engineering Department, Institute of Engineering and Technology, Lucknow, Sultanpur, India*
satyendrasingh@ietlucknow.ac.in

Abstract-- This paper presents the complex reliability of the PV and the wind power system linked to the grid. The power provided by a wind turbine is designed to suit the linear induction generator. The Archimedese wave swing (AWS) theory is used for the induction generator. A typical connection from dc bus bar through the voltage source converter connects the output terminal of the hybrid system (VSC). This dc power is therefore transformed into ac power by the inverter of the voltage source (VSI).. In order to smooth the rib, the electricity supplied to the power grid of the distribution side is indicated by a supercapacitor (SC). This paper suggests a control system to maintain the equilibrium between the distribution network's generated side and grid. To achieve the purpose, the traditional stabilization tool is added to the device under different conditions and approves the efficiency and performance of the topology used for control and the hybrid photovoltaic and wind turbines.

Index Terms--time-domain simulations, dynamic stability, photovoltaic array, linear permanent-magnet generator, root-loci analysis, super-capacitor supply power grid.

Introduction

Due to the expansion of the load requirement of a generation system and the impact of natural consequences[1]–[3], the usage of non-renewable energy sources such as charcoal, gas and so on is growing increasingly in current years. The oil products which degrade because the following decades will not be inexhaustible. The public modernisation is gradually growing the interest in energy development amid the existence of hybrid sources.. The primary arrangement to fulfil this demand requirement is to use affordable, renewable energy sources[4]–[7]. From various texts on photovoltaics and wind power, 56% of wind energy and 22% of Indian solar energy supplies were generated as of May 18, 2018 by a major factor in cultivating renewable sources of energy and interlinking it in the grid[8]. Mainly since mutual accessibility and solar power plant output regulation rely on individual sound accessibility and wind speed[10], solar and wind power generation has been increased. As sustained sources of energy have a high impact on the atmosphere, the voltage from sources is discontinuous or intermittent. To promote this, energy sources combine in order to define the network of renewable resources and MPPT control computers are required to track the most exceptional energy sources[11]. The fundamental form of a hybrid energy topology for renewable energy can be found in Fig.1. Other studies in MPPT include: dislocated and tracked (P&O), climbing, management of blurry, hybrid system and artificial neural grids open to optimising the energy independence from renewable sources[12]. In comparison, the development of the latest large independent wind-photovoltaic system[11] showed a design and style optimising approach to the new Voltaic Power Generation System with grid-connections based on the multifaceted innate algorithm. The unit was a stand-alone hybrid power generation system for photovoltaic batteries. In the new PV diesel power station, which uses a more wave in the PV handle curve, the dynamics stability of a macro grid that links to a wind transformer, the simultaneous diesel dynamo and a cellular energy storage repository were investigated[22], while fewer wave solidity production findings were presented at the new HPGS networked power station.. In [14], the developers suggested a narrative hold-strategy focused in particular on the charging conditions associated with the battery to increase the performance of photovoltaic and wind energy with the HPGS battery. In [15] the energy stabilisation of a hybrid macro grid with Super Capacitors has been documented[16] that the use of a small enterprise to increase the complex certainty of the grid-affixed wind power generating system throughout the matrix power plant. It has to be taken into account that almost all the proposed HPGSs announced in publications were mostly wind plus PV based. The fact that wind and PV will complement the other one is the outcome, and the technologies they share can be persuasive. . It is already mentioned that ocean energy will grow a significant segment of static technology in the years to come. Wind energy is typically the key to all of the generating solutions that are currently possible in relation to extreme potential stability, including the generation of electricity[18]-[21], such as wave movement, ocean power, etc. Wind power is generally the key. Though several excellent analyses have been conducted and detailed inside the WPG process (Wave Power Generation Systems) [17]-[29], the mixing of wind generating systems with the other RES systems in standard HPGSs has not been thoroughly investigated recently. In relation to hybrid power generation systems along with wind power, only a few more articles have in particular been published [30]-[32]. The authors in [32] extended the Photovoltaic-wave autonomous hybrid structure of renewable energy origin for Malaysia's islands. In this fusion experiment, a permanent magnet synchronous generator was reproduced by WPGS, powered by a travelling aqua up righteous unit and the cell boundary was used as a power-depot reinforcement order. In this article, energy stable effects are studied in respect to smoothing the power variations of a current matrix-related wind and photovoltaic HPGS. We propose a new control technique for the refinement of the force of the matrix, also to begin the balanced work of the system considered, while extracting the highest intensity from the wave along with the exhaustible means for PV. Usually, the layout of the researched scheme and the performance in the SC combined in accordance with the power structure given would be examined on the root-loci survey outcomes for the intrinsic importance of the operation, besides the initial steps. Segment III addresses the control function for the proposed topology. The findings of the simulations of implied topology in the time sector and its stability analysis are correspondingly seen in segments IV and V. Finally, section VI demonstrates the major findings of the paper.

Process Layout and Numerical Structures

a) Arrangement of the Designed Model

The structured model of the hybrid system connected to the grid is shown in Fig.1. The wind and photovoltaic system of are connected to the grid of distributed network. The wind power and PV system are interconnected to a voltage source converter (VSC) via dc/ dc step-up converter. The dc power delivered from VSC is interfaced to the grid through voltage source inverter. The step-up converter connected to the PV module consist MPPT tracking algorithm. The wind power generation system is based on linear permanent magnet generation system. Its basic operation is designed on Archimedes wave swing (AWS). Though the power delivered to the grid via hybrid system is fluctuating in nature, a supercapacitor (SC) is used to minimise the ripple [35]-[37]. The material used for constructing the supercapacitor has such characteristics a high longevity, quick repose time, high power density and does not require any cooling system. The supercapacitor also maintains balanced operation of the suggested topology , so that the interconnected converter and inverter can perform smoothly. The control mechanism for the suggested topology is presented in the next segment.

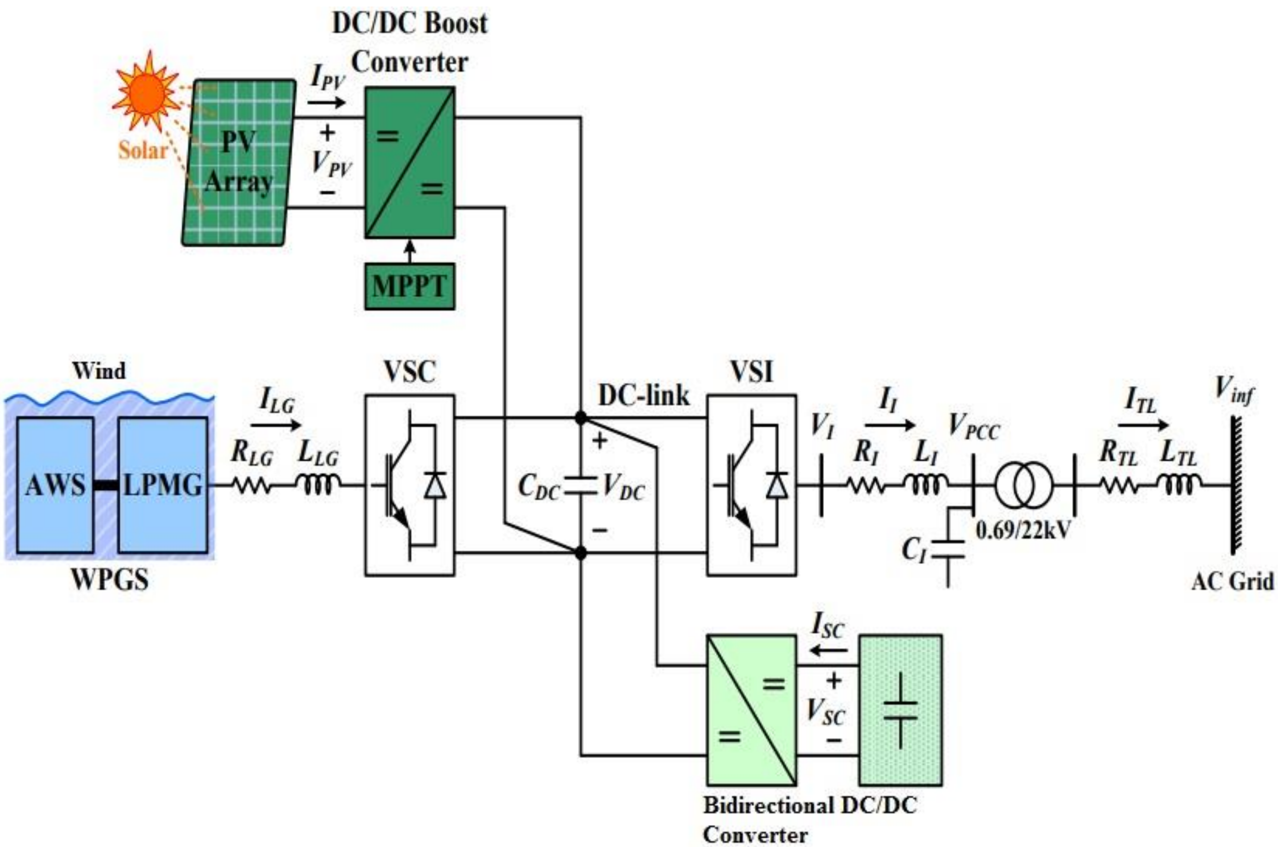

Fig.1 Schematic design of the PV and Wind system connected to the distribution grid

b) Representation of wind power generation systems

The AWS based wind power generation system explain the mechanical arrangement of the system. The mass- spring - damper [22] can be modeled as:

$$p(z) = uz \tag{1}$$

$$(m_t)p(u_z) = F_{wave} - K_{Sz} - K_D u_z - F_{LG} \tag{2}$$

here the gear operator is symbolized by p about time and the floater speed is denoted by z and U_z as well as the distances, correspondingly; m_t is the particular overall size of the specific floater as well as the L_{PMG} translator; F wave is the certain power coming from the wind, F_{LG} is the pressure performing on the floater; and K_D along with K_S are the dissipating ratio and spring consistent from the AWS, correspondingly. The particular L_{PMG}'s representation based upon the dq-axis mention of fixture set in the translator is documented by [18], [23], [29]:

$$(L_{dLG})p(i_{dLG}) = \omega_z L_{qLG} i_{qLG} - R_{LG} i_{dLG} - v_{dLG} \tag{3}$$

$$(L_{qLG})p(i_{qLG}) = \omega_z \psi_{PM} - \omega_z L_{dLG} i_{dLG} - R_{LG} i_{qLG} - v_{qLG} \tag{4}$$

exactly where i_{dLG} and i_{qLG} (v_{dLG} and v_{qLG}) are both the d and q-axis potentials (voltages), individually; R_{LG} will be the stator-winding resistance, L_{dLG} plus L_{qLG} would be the d plus q-axis simultaneous inductances, individually.

C) Representation of Photovoltaic with the step-up chopper

The Photo Voltaic module is made up of various Photo Voltaic segments interconnected in sequences. Every Photo Voltaic component is initiated by the variety of Photo Voltaic cells linked in sequence. Fig.2 displays the sole-diode comparative-circuit unit of the Photo Voltaic cell [38]-[42] that is composed of the power supply I_{ph}, a diode D_j, a parallel resistance R_p, and a sequence resistance Rs. By increasing the unit of a Photo Voltaic cell to characterize a PV range is shown within [40], [41], the resulted current (in A) of the analyzed Photo Voltaic range is indicated by

$$I_{PV} = N_{mp} I_{ph} - N_{mp} I_0 \left\{ \exp\left[\frac{q(V_{pv} + R_{sa} I_{pv})}{kATN_s Nms} \right] - 1 \right\} - (V_{pv} + R_{sa} I_{pv}) / R_{pa} \tag{5}$$

in which V_{PV} is the result voltage (shown as V) regarding the Photo Voltaic range; N_{ms} and N_{mp} are typically the figures of PV units attached in lines as well as in parallel, individually; N_s is the amount of the sequences-linked cells in a Photo Voltaic module; R_{sa} and R_{pa} are the similar collection and parallel resistances of the photovoltaic range, correspondingly; and I_{ph} and I_0 are the particular PV and invert saturation currents(in A), respectively. The particular currents I_{ph} and I_0 get as given [41]-[43]:

$$I_{ph} = \left[I_{sc,n} + k_i (T - T_n) \right] (G / G_n) \tag{6}$$

$$I_0 = I_{0,n} (T / T_n)^3 \exp\left[(qE_g / kA)(1 / T_n - 1 / T) \right] \tag{7}$$

In which

$$I_{0,n} = I_{sc,n} / \left\{ \exp\left[(qV_{oc,n}) / (kAT_n N_s) \right] - 1 \right\} \tag{8}$$

Exactly T and G will be working inversion (in K) and photovoltaic radiation (within W/m2), individually; I_{sc}, plus and Voc, n will be the limited-circuit power (within A) and unfold-outlet volt (in V) within regular analyzed situation of G_n =2000 W/m2 and T_n = 308. 14 K (35 ^{0}C); I_0, and is the invert saturation power at T_n; is limited-turn offered ratio (within A/K); For instance, the particular space energy associated with the semiconductor (within e_V); q,k, and also A would be the charge of electron (within C), the Boltzmann constant (within J/K), in addition to the diode ideality element, correspondingly. Fig. 3(a) displays the particular simplified plan through the analyzed dc/dc enhance converter about interconnecting the Photo Voltaic range to the dc connection. Suppose the thorough transforming behavior of the diode D and the switch S proven in Fig. 3(a) are overlooked. The particular dc/dc enhanced converter may be displayed by the particular powerful typical-value unit since tested within Fig. 3(b). Hence, the dynamic calculation utilized to simulate the particular dc/dc enhanced converter can be acquired through [43],[44]:

$$(C_p)p(V_{PV}) = i_{PV} - i_{LP} \quad (9)$$

$$(L_P)p(i_{LP}) = -R_P i_{LP} + V_{PV} - (1-D_P)V_{DC} \quad (10)$$

$$i_{PV\_DC} = (1-D_p)i_{LP} \quad (11)$$

wherever C_P is typically the filter capacitor; L_P and R_P are the particular certain inductance and host stage of resistance-associated together with the power-save keeping inductor coming from the converter, correspondingly; it may be the inductor current; I_{PV_DC} may be the particular current provided towards the particular dc power link from the enhanced converter; V_{DC} could be the dc-link electricity; in addition to this, D_P will be the liable ratio from the current dc/dc enhanced converter.

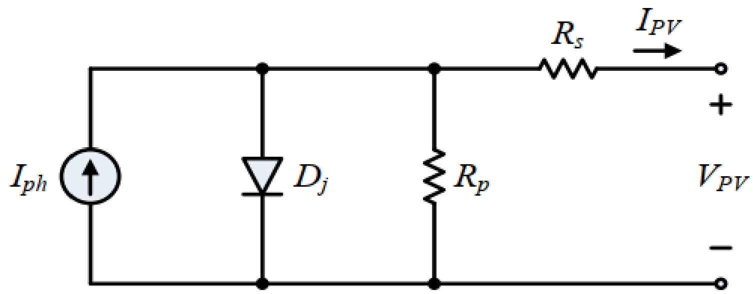

Fig. 2. Circuit of standalone photovoltaic cell

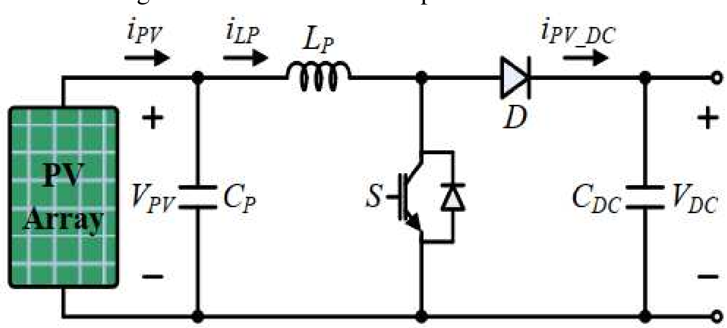

a

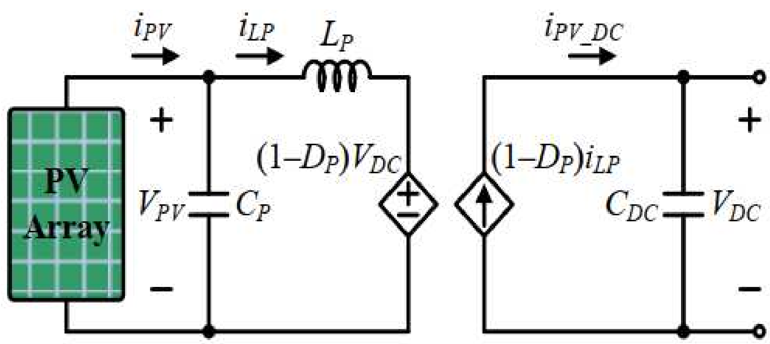

b

Fig. 3. (i) Equivalent circuit diagram and (ii) dynamic logic diagram

.

D. *Depiction of SC and DC-DC Converter*

Fig.4 demonstrates the similar-circuit unit of researched Super Capacitor as [45]. In inclusion to the capacitor C_{SC} of the Super Capacitor, the following representation as well holds into consideration the reduction of Joule as well as self-applied-release occurrence of the Super Capacitor, that are displayed by the aversion to R_{pSC} and R_{pSC}, correspondingly. With reference on Fig.4, [46] acquires the related dynamic calculations of the used Super Capacitor.

$$(C_{sc})p(V_{csc}) = -i_{sc} - V_{csc} / R_{psc} \tag{12}$$

$$V_{sc} = V_{csc} - R_{qsc} i_{sc} \tag{13}$$

Where V_{SC} and i_{SC} are the current and power of the Super Capacitor, individually; whereas V_{CSC} is the voltage across over C_{SC}.

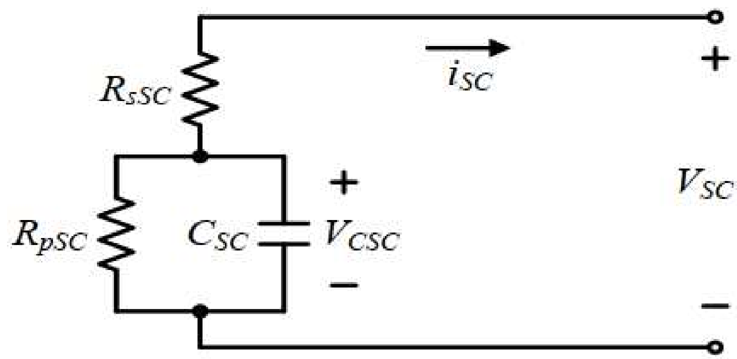

Fig. 4.Equivalent circuit of a supercapacitor.

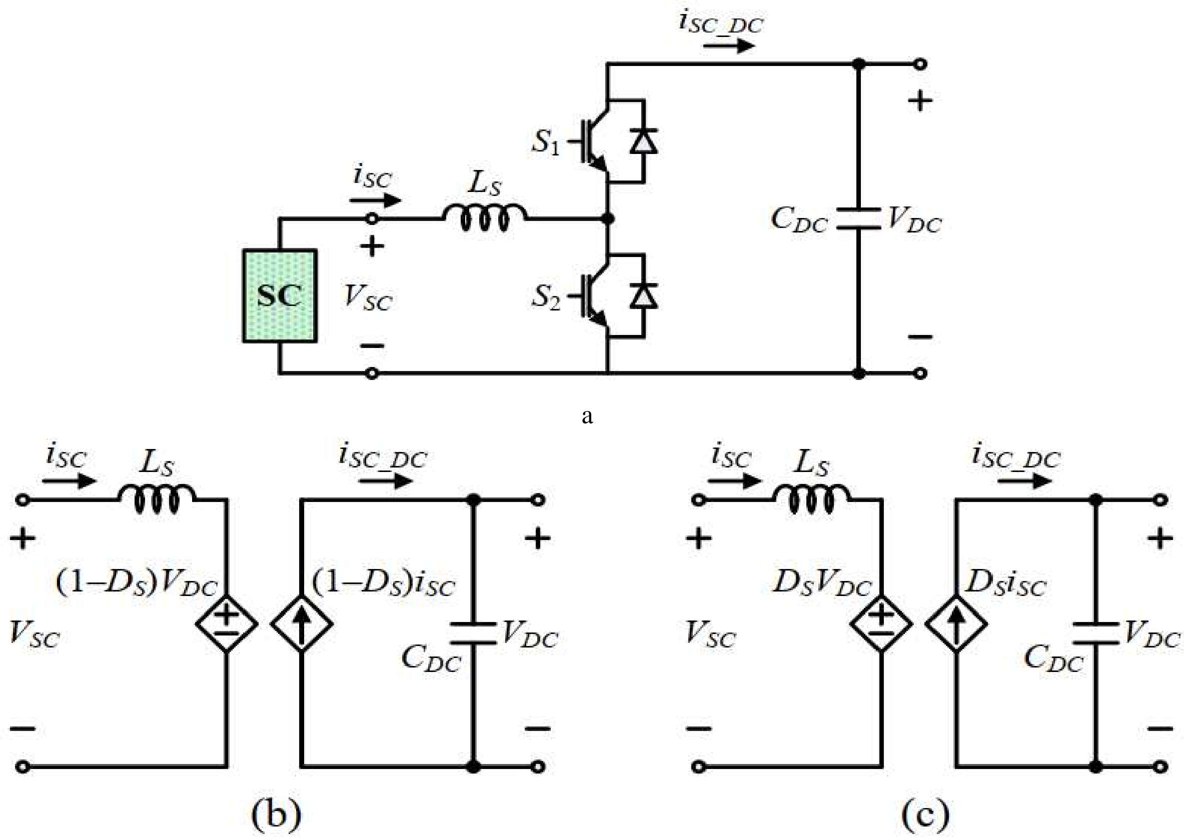

Fig. 5 Basic presentation of the back to back dc/dc converter

Fig.5(a) displays the simplified layout of the used biface dc/dc enhanced converter for combining the Super Capacitor into the dc connection. The minimal-current position of the biface dc/dc enhanced converter is associated to the Super Capacitor linked to the dc connection. The converter is composed of a couple of switches S_1 and S_2 that are controlled in a supporting approach together with power-storage inductor L_S. This particular setup permits the attribute of the biface current circulation of the converter. In buck setting of procedure, the switch S_1 serves as a switch whereas S_2 serves like a diode [47], and the current passes via the dc connection to the Super Capacitor. On the other hand, within the boost setting of procedure, the switch S_2 works like a switch whereas S_1 works as a diode and the energy runs by the Super Capacitor to the dc connection. Likewise, once building the dc-dc converter in supercharged condition to the prior subsection, the comprehensive transitioning ways are usually overlooked. Hence, the biface dc-dc enhanced converter could be simulated with the use of its dynamic mean-value unit. Fig.5 (b) and Fig.5(c) describes the active mean-value of biface dc-dc enhanced topology has great function and the step-down setting of procedure, correspondingly. Below are the dynamic calculations about these two methods of operation.

a) Boost mode:

$$(L_s)p(i_{sc}) = -R_s i_{sc} + V_{sc} - (1 - D_s)V_{DC} \tag{14}$$

$$i_{SC-DC} = (1 - D_s)i_{sc} \tag{15}$$

b) Buck mode:

$$(L_s)p(i_{sc}) = -R_s i_{sc} + V_{sc} - D_s V_{DC} \tag{16}$$

$$i_{SC-DC} = D_s i_{sc} \tag{17}$$

exactly where L_S and R_S would be the inductance as well as parasite level of resistance of the power-storage inductor, individually; i_{SC_DC} here becomes the particular power in the dc-link part.

E. Arrangement of Voltage-source Inverter

The particular VSI, as proven within Fig.1, which is linked into the circulation energy grid with an LC filtration system, a networked line, a stage-up transformer. The particular dynamic units of all these types of elements within the axis research figure can be documented as:

$$(L_I)p(i_{dI}) = -R_I i_{dI} + \omega_e L_I i_{qI} + \upsilon_{dI} - \upsilon_{dPCC} \tag{18}$$

$$(L_I)p(i_{qI}) = -R_I i_{qI} - \omega_e L_I i_{dI} + \upsilon_{qI} - \upsilon_{qPCC} \tag{19}$$

$$(C_I)p(\upsilon_{dPCC}) = i_{dI} - i_{dTL} + \omega_e C_I \upsilon_{qPCC} \tag{20}$$

$$(C_I)p(\upsilon_{qPCC}) = i_{qI} - i_{qTL} - \omega_e C_I \upsilon_{dPCC} \tag{21}$$

$$(L_{TL})p(i_{dTL}) = -R_{TL} i_{dTL} + \omega_e L_{TL} i_{qTL} + \upsilon_{dPCC} - \upsilon_{d\inf} \tag{22}$$

$$(L_{TL})p(i_{qTL}) = -R_{TL} i_{qTL} - \omega_e L_{TL} i_{dTL} + \upsilon_{qPCC} - \upsilon_{q\inf} \tag{23}$$

where (V_{dI} and V_{qI}) and (i_{dI} and i_{qI}) are the result electricity and powers of the VSI; (v_{dPCC} together with v_{qPCC}) and (v_{dinf} together with v_{qinf}) are the powers of the very level of frequent coupling (PCC) along with the circulation energy main grid, correspondingly; (i_{dTL} and i_{qTL}) are usually the energies of the interconnection range.

Control Methodology

This section illustrates the control function of the proposed topology. Its key goal is to reduce energy supply rips and grid noise in order to protect the stability of the network. The PV module and the wind power can be accomplished by correctly controlling the dc / dc step-up controller and the VSC. The power supply to the grid is regulated by a VSI controller, while the dc side voltage is maintained by the bilateral dc-dc. The thorough analysis of the system of control is discussed:

1. Control mechanism of step-up Converter for the Photo Voltaic Range

The PV module's power fluctuates and varies with the irradiance. The full capacity of the PV module must always be controlled in order to operate the system efficiently. To achieve this purpose, the PV module-associated step-up dc-dc converter can be operated to control the module's output voltage in order to achieve the appropriate maximum value. Various MPPT algorithms are suggested in literature. In addition P&O is used to monitor the operation of the step-up dc-dc converter.

2. Control mechanism of WPGS for VSC

The control strategy for individual VSC is seen in fig.6. The proposed d & q axis figure subjected to the basic LPMG translator is adjusted in the VSC-associated operator. The unique WPGS should be allowed to receive the maximum energy from the wind as well as to lower the energy reduction in the LPMG. In [23], the energy loss and productive wind converted energy can be seen in the individual LPMG as well as by the LPMG d&q axis (idLG and iqLG), individually. As proven in Fig.6, the provided control structure associated with the VSC, makes the use of PI remotes to determine the d-q axis powers of L_{PMG} to typically the research index (i_{dLG_ref}) in addition to (i_{qLG_ref}).

$$i_{qLG\_ref} = (2\tau K_D U_z) / (3\pi \psi_{PM}) \tag{24}$$

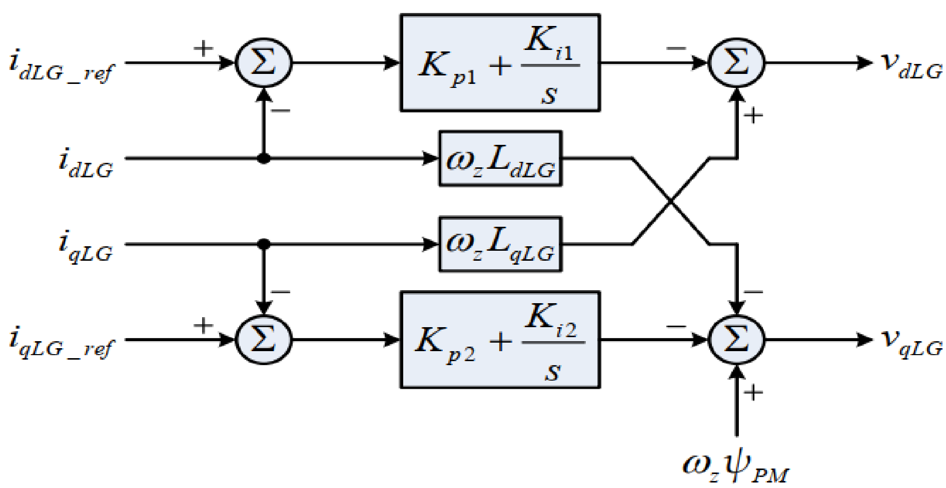

Fig. 6. Representation of control blocks used for design of WPGS.

The structure of the VSI is seen in Fig.7. The VSI-related controller can be used to handle the output energy transferred through the VSI and to preserve the PCC's volts value for the research value. The power over the relevant VSI is obtained by using the d-axis axis lined up to the PCC volts vector, in order to gain a dissociated control connected with the active and reactive components. In this case As a consequence, d-q axis forces for specific VSI (IdI and iqI) are respectively administered for efficient energy transmitted through the inverter of the voltation source connected with the PCC. The VSI-associated controller, as shown in Fig. 7 provides the rapid method in which external management loops handle the effective energy transmitted from VSI at the specific voltage..

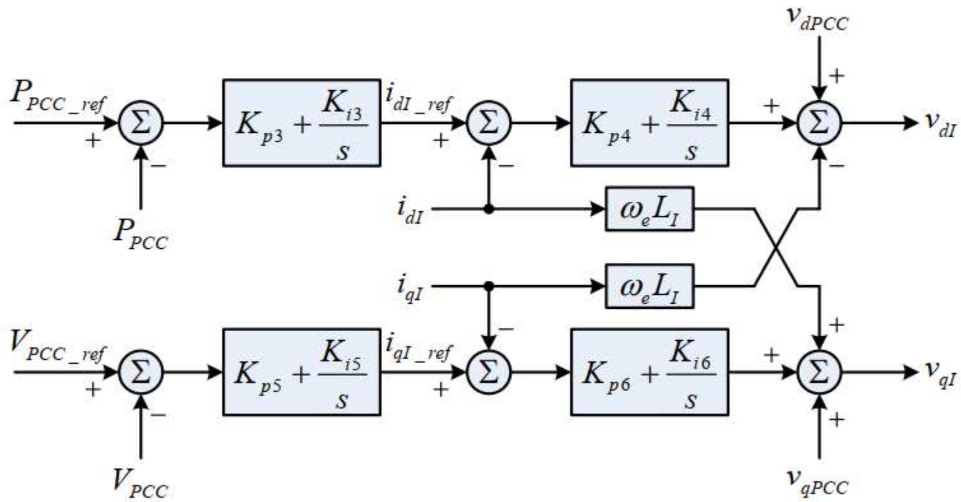

Fig. 7.VSI block mechanism.

In order to allow the VSI to seamlessly shift the power generated by the PV, the PCC ref of pV and wind power generation systems can be transferred through the reference point of the active power movement through the VSI. The scheme as presented in Fig.8 can be used to do this. The hybrid system's built power is transferred by the low-pass filter (LPFs). As seen in Fig.8, T1 and T2 symbolise the low pass time constant. In order to minimise the difference in wind capacity, T1 equal to the Tw wind length should be used. The other constant, however is that T2 can be selected to monitor the high frequency of power of the PV module.

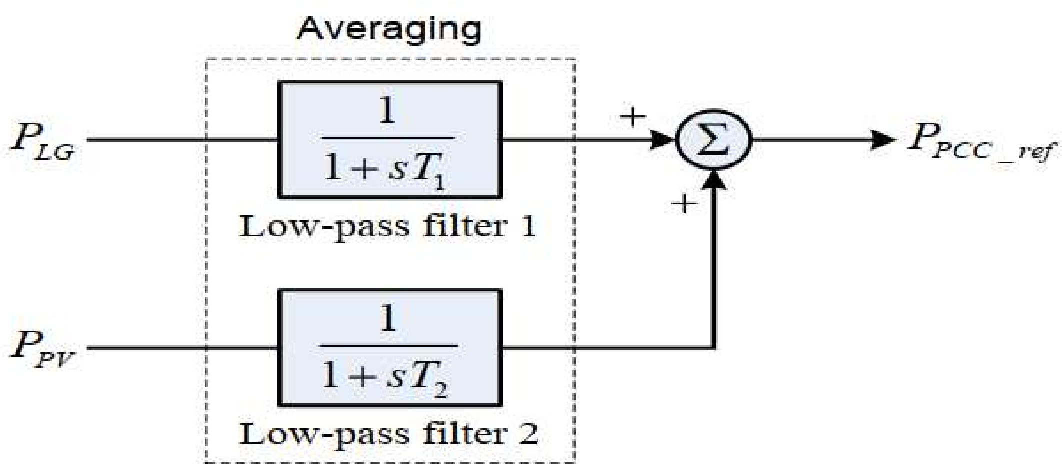

Fig. 8.Resolution of the mention of value (*PPCC_ref*)

3. Manage of Biface dc-dc enhanced topology for Super Capacitor

Fig.9 sets up the control of the block structure of an usually bilateral dc-dc-enhanced converter from which the Super Capacitor is attached to dc. In general, the controller of the improved bilateral dc-dc converter relies on a range of approximate management loops released. The external control cycle usually retains the VDC connection volts while the VDC refer is noted and the internal control cycle administers the power inside a SC iSC. When the dc-connection volt quality is withdrawn from the guide value, the current is generally controlled by the Super Capacitor to the guiding value iSC ref created by the external control cycle.

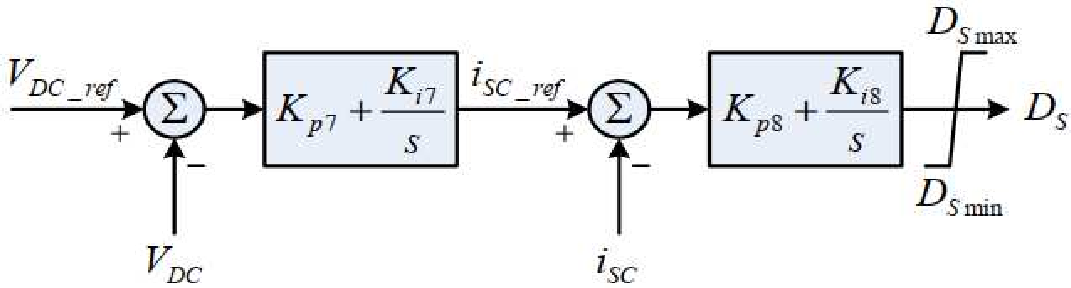

Fig. 9. structural layout of the control bi facing dc-dc converter.

Determination of Eigenvalues and Root-Loci

1. Method Eigen-values

Fig.1 offers an uncommon view of the studied wind and photovoltaic system below the selected operating point, at which solar radiance and wave force are typically measured individually at their optimum 1000 W/m2 values along with 0.9 MN. Although in comparable times certain especially successful circumstances of photovoltaic irradiance and wave pressure frequently do not exist, it is worth evaluating the process properly within most critical energy flows..

The eigenvalues and irradiance of solar for 1000 W/M2 and wind force 0.6 MN

Step no.	Eigen-values	Step no.	Eigen-values
Λ_{1-2}	$-118.8020 \pm j24.7874$	Λ_{15-16}	-0.22647; -1337.4160
Λ_{3-4}	$-160.5717 \pm j4988129.7394$	Λ_{17-18}	-204.3407; -497.0582
Λ_{5-6}	$-160.6133 \pm j4987450.1432$	Λ_{19-20}	-0.7989; -1.5997
Λ_{7-8}	$-687.5884 \pm j299.0561$	Λ_{21-22}	$-693.6852 \pm j1232.9736$
Λ_{9-10}	$-493.8432 \pm j232.0693$	Λ_{23}	-3621.7926
Λ_{11-12}	-9.7558; -9.6453	Λ_{24-25}	-0.1518; -0.2000
Λ_{13-14}	-0.3504; -1.2751	Λ_{26-27}	-114.6574; -20372.6950

Here, 27 eigenvalues of the particular analyzed technique detailed within Table I. The eigenvalues Λ 1-14 connect with the manage modes from the VSI together with the methods from the electric power connections amid as part of the VSI. The particular eigenvalues Λ 15- Λ 20 directs to the modes of the specific wind power generating system as well as the management stages for VSC. The particular eigenvalues Λ 24- Λ 27 associate to the ways from the Super Capacitor in addition to the dual modes of dc/dc converter. This will be observed that most of the eigenvalues outlined in Fig.10 has unfavorable actual components, which implies that the particular examined method is steady within the given functioning stage.

2. Study of Root-Loci

The underlying methodology on the basis of root values, i.e. root-loci dependent on the PV-range irradiation, is increased by 0 to 500 W/ m2 in Figure 10. Figure 10 In addition the wind power performed under the WPGS AWS concept is set to

0. Five MN. It should be remembered that the underlying root loci of the own values 21-22 that associates to a basic dc-dc step-up converter connecting the PV module is one of the most noticeable movement. Consequently, the margin of stability of the proposed system could be expanded due to solar expansion.

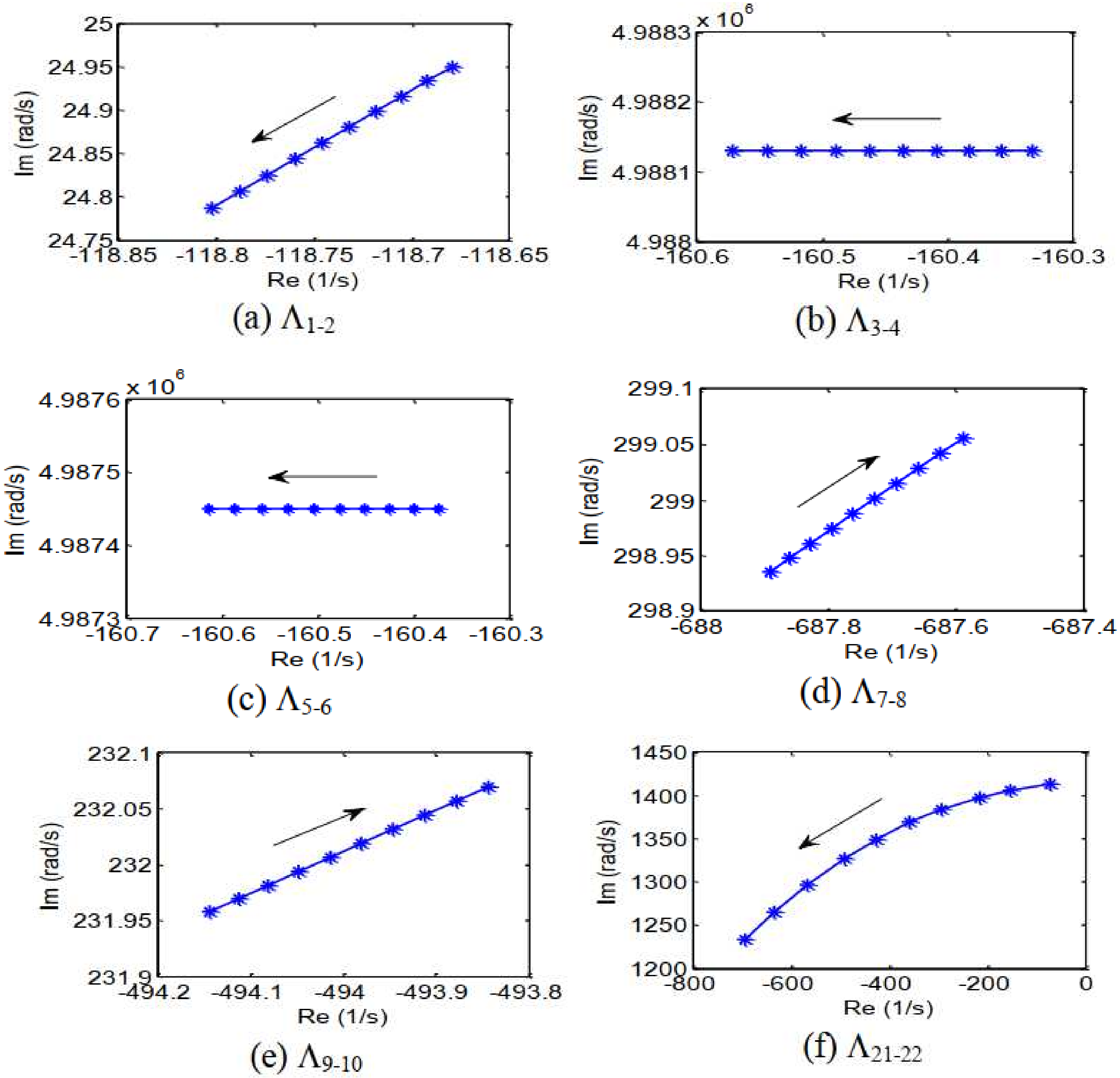

Fig. 10. Illustration of root-loci based on suggested technique based on eigenvalues up to 500 W/m^2.

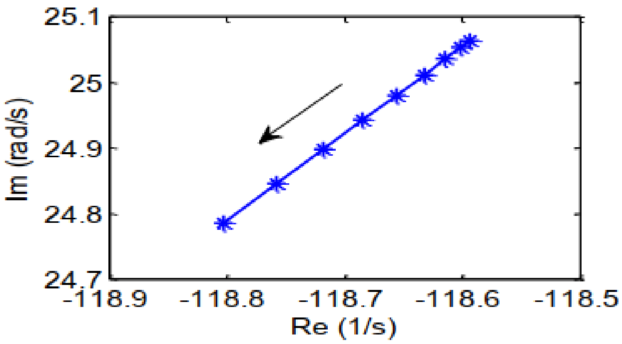

(a) $\Lambda_{1\text{-}2}$

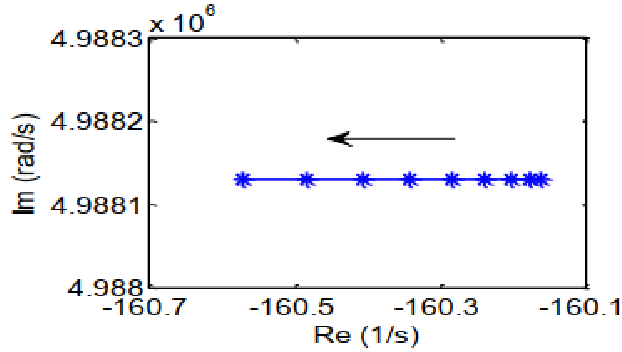

(b) $\Lambda_{3\text{-}4}$

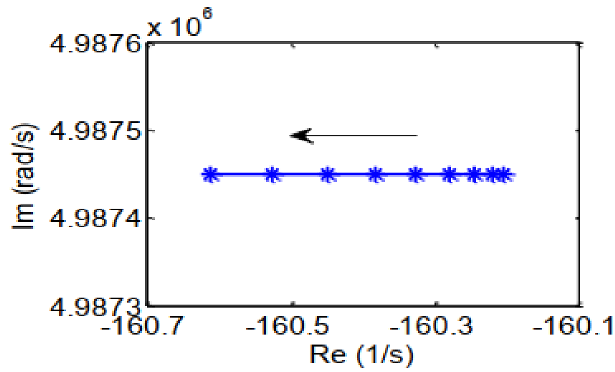

(c) $\Lambda_{5\text{-}6}$

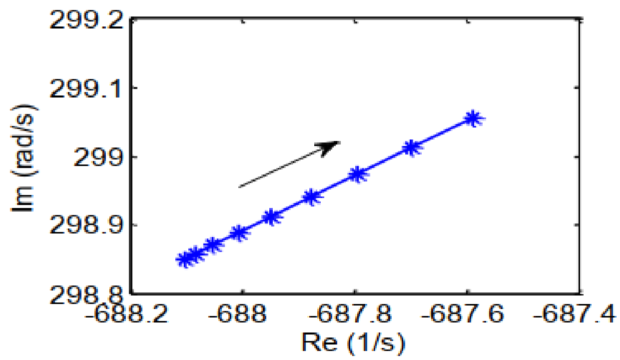

(d) $\Lambda_{7\text{-}8}$

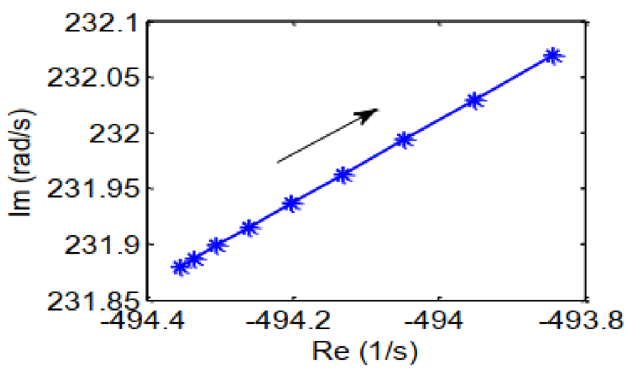

(e) $\Lambda_{9\text{-}10}$

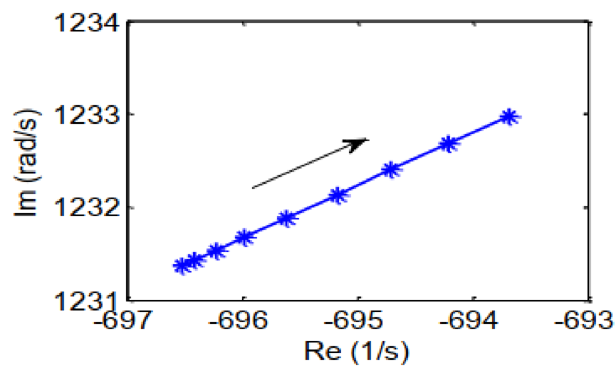

(f) $\Lambda_{21\text{-}22}$

Fig. 11 Root-loci of the wind energy acting upon the WPGS

Fig.11 demonstrates the stability analysis of root loci. Therefore, with the rise in wind energy, the dissipating attributes of modes are typically increased. In comparison, in general the patented values of 7-8, 9-10 are also strengthened on 21-22 as the wind pressure increases and when the basic dissipating efficacy of these mode forms is reduced as the wind energy grows. However, Fig. 11 revealed that, based on a basic left side on the complex stage, this analysed mechanism is reasonably steady within the wide range variants from wind energy within the fundamental root loci of the self-value procedure.

V. Analysis of Time-Domain

Case 1: Variants of the Wind Energy

The wind pressure from the AWS from the WPGS in this section was linked to the variations provided in Fig12 (a). In the versions dealing with wave energy, the active reactions of the analyses system are seen in Figs.12(b)-(c). The intensity and immediate energy of the individual AWS are continuously different due to the variants of the same wave energy as shown in Fig. 12(d). The rate of repeat of the speed reaction is the same since the wind-energy frequency while the repetition of energy emitted by the LPMG is two times the wind-energy-related frequency. The reactions calculated at different concentrations of the analysed phase, such as active energy from the main power grid, the PCC volts and power supply voltage, were shown in Figure 12(e)-(g). With this response one may find that the specific power variances of the wave variant can be regulated effectively when the analysed method is charged with the specific Super Capacitor, from transport to the particular power principal grid along with the dc-connection volt. In this case, as illustrated in the fig. 12 (h), the energy shifts are regulated by the Super Capacitor. In addition, when a Super Capacitor is devoid of the evaluated process, the energy changes attributable to the wind variants are turned around in the energy provided to the grid, whereas the dc connector volt is virtually stable at its considered value. It can clearly be inferred from the doubling of the findings that the Super Capacitor can effectively increase the overall functionality of the system studied in the variants of the specific wave energy behaviour on the AWS of the WPGS.

Case 2: Variants of Solar power Irradiance

The solar cell spectrum photovoltaic radiance, as seen in Fig.13(a), in this particular section is derived when the maximal amplitude of the wave energy, combined with an interval of 10 seconds, is sustained at 0.4 MN. The variants of solar energy radiation should also consist of significant imbalances in stability as local environmental patterns are rapidly evolving.

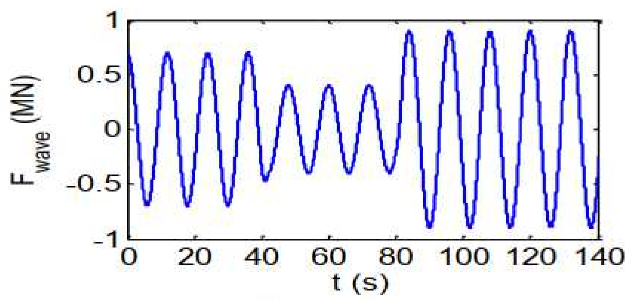

(a) Wave force

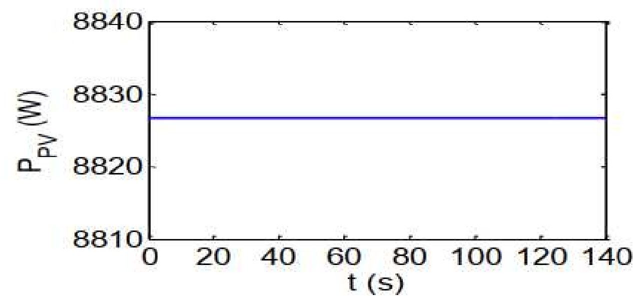

(b) P_{PV}

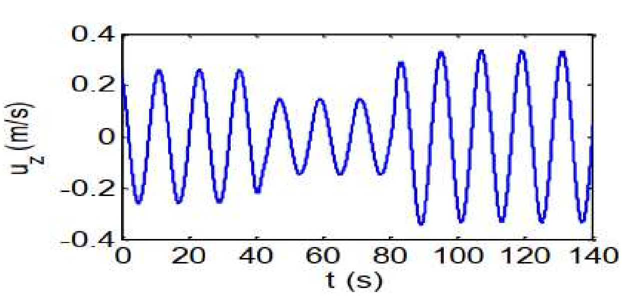

(c) u_z

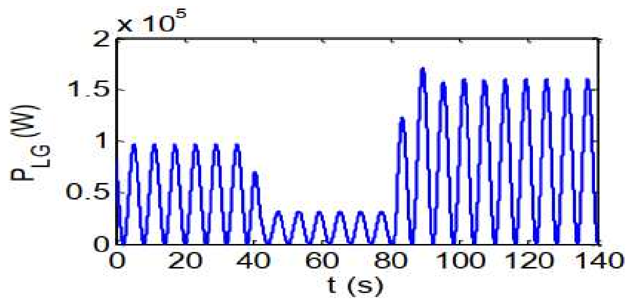

(d) P_{LG}

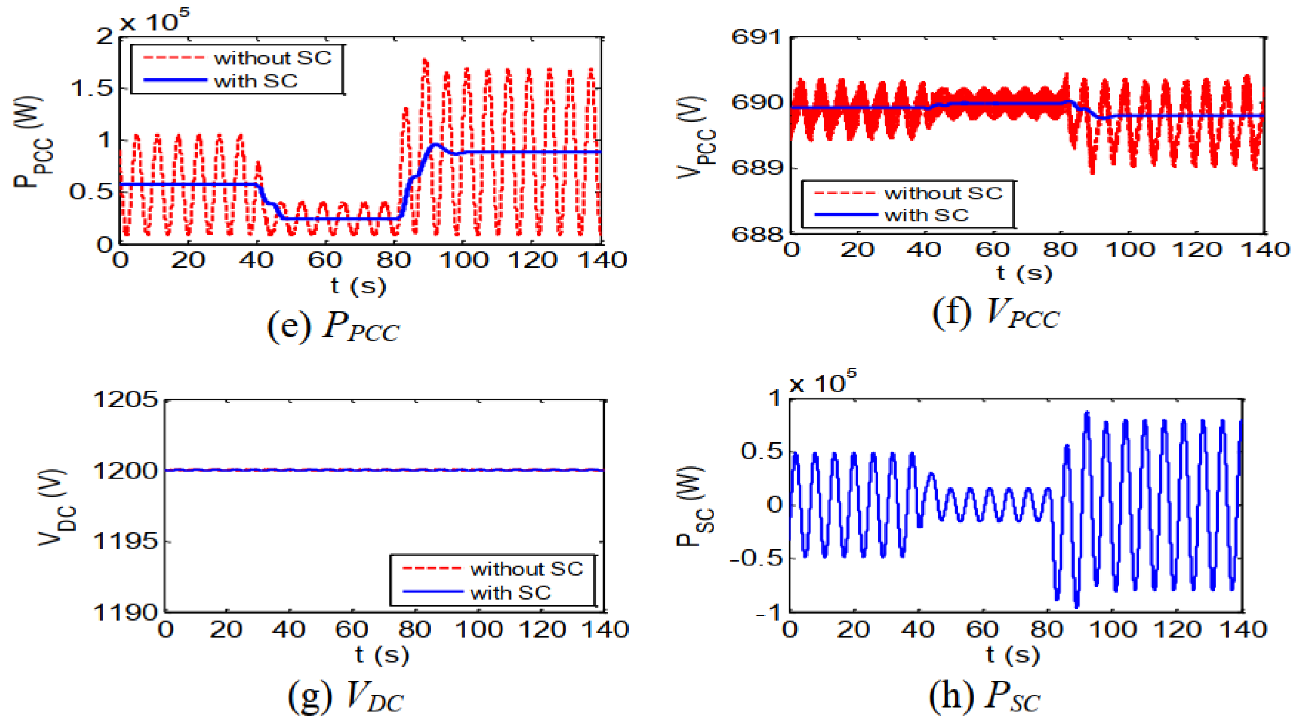

Fig. 12. Active reactions of the analyzed method within the variants of the wind energy

The dynamic response of the photovoltaic energy provided by the photovoltaic module with LPMG is presented individually in Fig.13(b). Fig.13 (b) states that the resultant energy of the photovoltaic module modifies the radiation increase and decrease in solar energy, and reveals the excessive-regular variances in solar energy radiation. Also noted in Fig.13(c) is that the output of the relevant LPMG's energy does not have any effect on the power variants obtained by solar radiation and its maximum value is typically only about 10 kW because the wind energy's high strength is only relatively small. Fig. 13(d)-(e) shows, together with and without Super Capacitor, the relative reactions of the energy given throughout the power grid with the dc communication volts of the researched process. This implies, that the productive energy supplied to the power grid is reasonably simple and the volt dc could be handled at the value considered if the studied system is developed along with the Super Capacitor. The unique overdue energy variations provided by the Photo Voltaic range were assimilated with the super capacitor as shown in Fig13 (f).

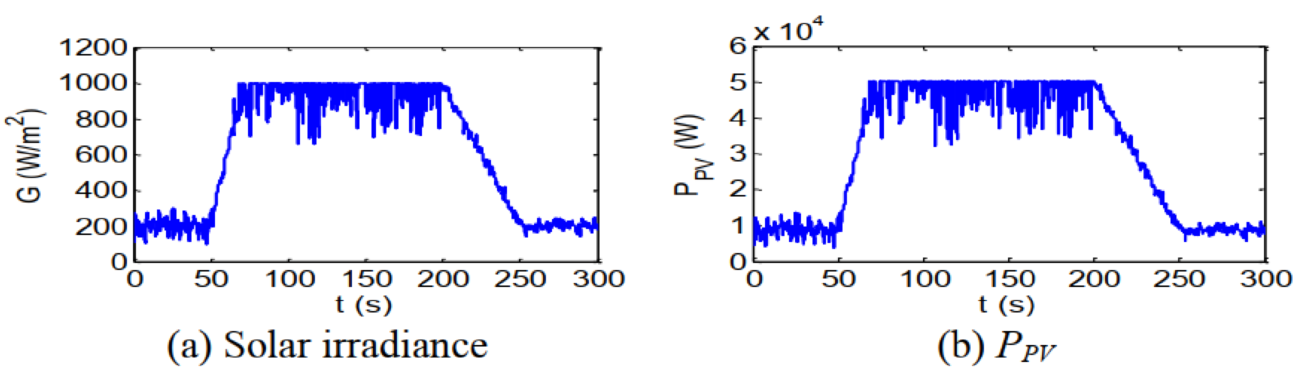

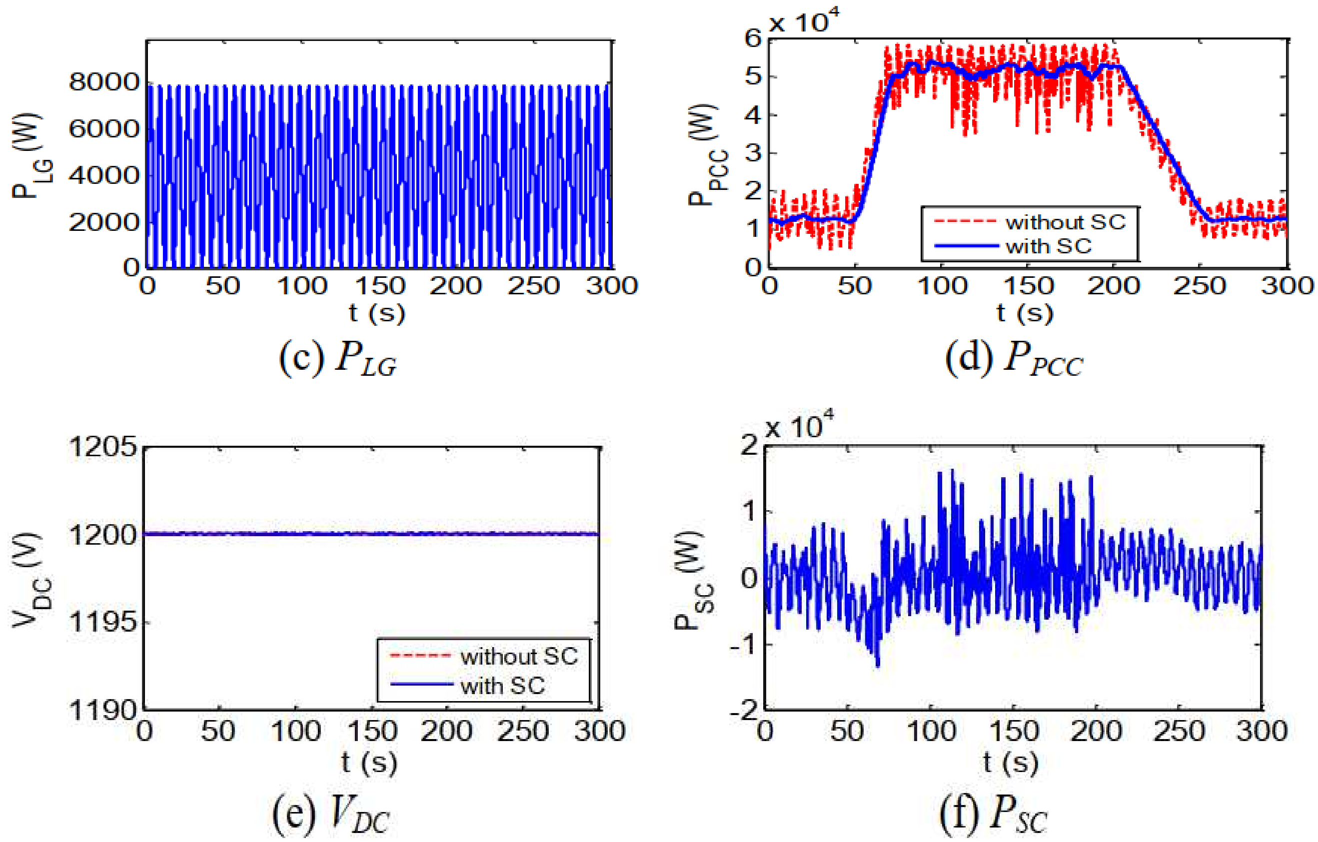

(c) P_{LG} (d) P_{PCC}

(e) V_{DC} (f) P_{SC}

Fig.13. Active reactions of the analyzed method within the variations of the solar power

Case 3: Result of the area of the Utilized SC

Here the data on the efficacy of the system analysed are determined by the scale of the Super Capacitor used. In addition to the energy measurement of 60 kW, 30 kW and 95 kW, roughly three separate Super Capacitors are typically in turn used for the analysed process. Fig.14 displays the relative complex energy reactions to the power supply main grid with around three different Super Capacitor energy assessments. This can be shown in the plots seen in Fig.14 because once the size of the Super Capacitor used is improved, the energy given to the main power supply system is finer. This is an indication of the additional development of the reliability of the analysed process if the Super Capacitor is used larger.

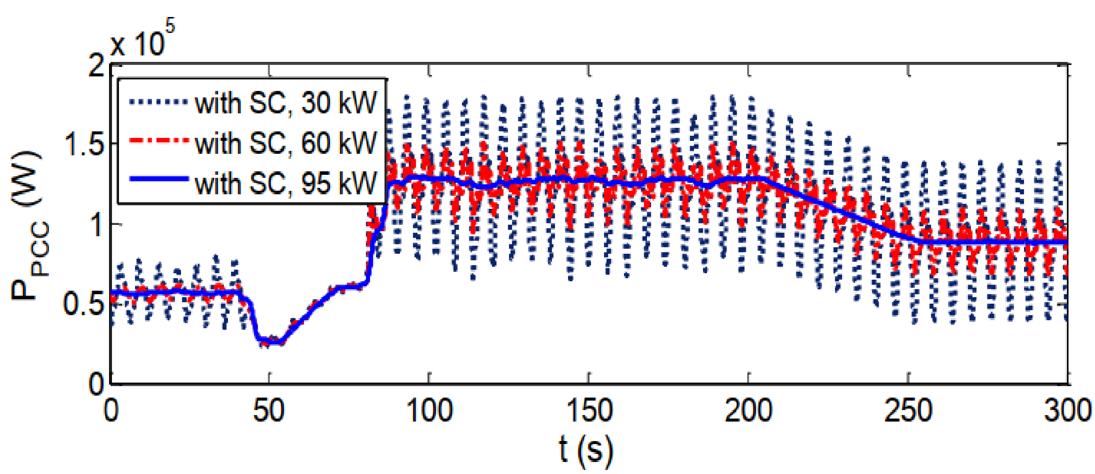

Fig. 14. Comparative dynamic reactions of the effective energy given to the distribution energy main grid for various energy classification of the utilized SC

Conclusion

A detailed analysis was undertaken concerning the reliability of the inter-grid hybrid PV and wind power system. To mitigate the fluctuation of the linked grid system the energy storage system on the supercapacitor is used. A control strategy is also recommended in order to retain the equilibrium process and gain optimum power from the hybrid grid-connected system. The system is evaluated both root and time domain to track dynamics under varying operating conditions. This system is used for complex efficiencies. The outputs of the proposed control technique can be summed up to sustain the function of the equilibrium of the described system.

Compliance with Ethical Standards

1. **Disclosure of potential conflicts of interest:** The authors declare that they have no conflict of interest.
2. **Research involving human participants and/or animals:** This paper does not contain any studies with human participants or animals performed by any of the authors.
3. **Informed consent:** Informed consent was obtained from all individual participants included in the study
4. **Funding:** This study was not funded by any agencies.

References

[1] Ge, X.-J., Sun, Y., Wang, Z.-H., & Tang, C.-S. (2019). A single-source switched-capacitor multilevel inverter for magnetic coupling wireless power transfer systems. Electrical Engineering. doi:10.1007/s00202-019-00850-5.

[2] S.-K. Kim, J.-H. Jeon, C.-H. Cho, J.-B. Ahn, and S.-H. Kwon, “Dynamic modeling and control of a grid-connected hybrid generation system with versatile power transfer,” IEEE Trans. Industrial Electronics, vol. 55, no. 4, pp. 1677-1688, Apr. 2018.

[3] X. Liu, P. Wang, and P. C. Loh, “A hybrid ac/dc microgrid and its coordination control,” IEEE Trans. Smart Grid, vol. 2, no. 2, pp. 278- 286, Jun. 2016.

[4] M. M. R. Singaravel and S. A. Daniel, “MPPT with single dc-dc converter and inverter for grid-connected hybrid wind-driven PMSG-PV system,” IEEE Trans. Industrial Electronics, vol. 62, no. 8, pp. 4849- 4857, Aug. 2015.

[5] Y. J. Reddy, Y. V. P. Kumar, K. P. Raju, and A. Ramesh, “Retrofitted hybrid power system design with renewable energy sources for buildings,” IEEE Trans. Smart Grid, vol. 3, no. 4, pp. 2174-2187, Dec. 2014.

[6] C. Wang and M. H. Nehrir, “Power management of a stand-alone wind/photovoltaic/fuel cell energy system,” IEEE Trans. Energy Conversion, vol. 23, no. 3, pp. 957-967, Sep. 2018.

[7] L. N. Khanh, J.-J. Seo, Y.-S. Kim, and D.-J. Won, “Power-management strategies for a grid-connected PV-FC hybrid system,” IEEE Trans. Power Delivery, vol. 25, no. 3, pp. 1874-1882, Jul. 2017.

[8] P. Garcia, C. A. Garcia, L. M. Fernandez, F. Llorens, and F. Jurado, “ANFIS-based control of a grid-connected hybrid system integrating renewable energies, hydrogen and battery,” IEEE Trans. Industrial Informatics, vol. 10, no. 2, pp. 1107-1117, May 2016.

[9] B. Liu, F. Zhuo, Y. Zhu, and H. Yi, “System operation and energy management of a renewable energy-based dc micro-grid for high penetration depth application,” IEEE Trans. Smart Grid, vol. 6, no. 3, pp. 1147-1155, May 2016.

[10] D. Abbes, A. Martinez, and G. Champenois, “Eco-design optimization of an autonomous hybrid wind-photovoltaic system with battery storage,” IET Renewable Power Generation, vol. 6, no. 5, pp. 358-371, Sep. 2016.

[11] M. B. Shadmand and R. S. Balog, “Multi-objective optimization and design of photovoltaic-wind hybrid system for community smart dc microgrid,” IEEE Trans. Smart Grid, vol. 5, no. 5, pp. 2635-2643, Sep. 2014.

[12] N. Patel, N. Gupta, and B. C. Babu, “Photovoltaic System Operation as DSTATCOM for Power Quality Improvement Employing Active Current Control,” *IET Generation, Transmission & Distribution*, May 2019.

[13] N. Patel, A. Kumar, N. Gupta, S. Ray, and B. C. Babu, “Optimized PI-4VPI Current Controller for Three-Phase Grid-integrated Photovoltaic Inverter under Grid Voltage Distortions,” *IET Renewable Power Generation*, vol. 14, no. 5, pp. 779-792, Nov. 2019.

[14] S. Mishra and D. Ramasubramanian, “Improving the small signal stability of a PV-DE-dynamic load-based microgrid using an auxiliary signal in the PV control loop,” IEEE Trans. Power Systems, vol. 30, no.1, pp. 166-176, Jan. 2018.

[15] X. Li, D. Hui, and X. Lai, “Battery energy storage station (BESS)-based smoothing control of photovoltaic (PV) and wind power generation fluctuations,” IEEE Trans. Sustainable Energy, vol. 4, no. 2, pp. 464- 473, Apr. 2016.

[16] S.-T. Kim, B.-K.Kang, S.-H.Bae, and J.-W. Park, “Application of SMES and grid code compliance to wind/photovoltaic generation system,” IEEE Trans. Applied Superconductivity, vol. 23, no. 3, pp. 5000804, Jun. 2018.

[17] J. Khan and U. Nasir, “Voltage stabilization of hybrid micro-grid using super capacitors,” J. Power and Energy Engineering, vol. 3, no. 6, pp. 1- 9, Jun. 2015.

[18] S. Ceballos, J. Rea, I. Lopez, J. Pou, E. Robles, and D. L. O’Sullivan, “Efficiency optimization in low inertia Wells turbine-oscillating water column devices,” IEEE Trans. Energy Conversion, vol. 28, no. 3, pp. 553-564, Sep. 2017.

[19] F. Wu, X.-P. Zhang, P. Ju, and M. J. H. Sterling, “Optimal control for AWS-based wave energy conversion system,” IEEE Trans. Power Systems, vol. 24, no. 4, pp. 1747-1755, Sep. 2019.

[20] Z. Nie, X. Xiao, R. McMahon, P. Clifton, Y. Wu, and S. Shao, “Emulation and control methods for direct drive linear wave energy converters,” IEEE Trans. Industrial Informatics, vol. 9, no. 2, pp. 790- 798, May 2018.

[21] L. Cappelli, F. Marignetti, G. Mattiazzo, E. Giorcelli, G. Bracco, S. Carbone, and C. Attaianese, “Linear tubular permanent-magnet generators for the inertial sea wave energy converter,” IEEE Trans. Industry Applications, vol. 50, no. 3, pp. 1817-1828, May/Jun. 2014.

[22] J. Prudell, M. Stoddard, E. Amon, T. K. A. Brekken, and A. von Jouanne, “A permanent-magnet tubular linear generator for ocean wave energy conversion,” IEEE Trans. Industry Applications, vol. 46, no. 6, pp. 2392-2400, Nov./Dec. 2018.

[23] H. Polinder, M. E. C. Damen, and F. Gardner, “Linear PM generator system for wave energy conversion in the AWS,” IEEE Trans. Energy Conversion, vol. 19, no. 3, pp. 583-589, Sep. 201

[24] F. Wu, X.-P.Zhang, P. Ju, and M. J. H. Sterling, “Modeling and control of AWS-based wave energy conversion system integrated into power grid,” IEEE Trans. Power Systems, vol. 23, no. 3, pp. 1196-1204, Aug. 2018.

[25] F. Wu, P. Ju, X.-P. Zhang, C. Qin, G. J. Peng, H. Huang, and J. Fang, “Modeling, control strategy, and power conditioning for direct-drive wave energy conversion to operate with power grid,” Proc. IEEE, vol. 101, no. 4, pp. 925-941, Apr. 2018.

[26] G. Brando, A. Dannier, A. D. Pizzo, L. P. D. Noia, and C. Pisani “Grid connection of wave energy converter in heaving mode operation by supercapacitor storage technology,” IET Renewable Power Generation, vol. 10, no. 1, pp. 88-97, Jan. 2019.

[27] M. Alberdi, M. Amundarain, A. J. Garrido, I. Garrido, O. Casquero, and M. D. la Sen, “Complementary control of oscillating water column based wave energy conversion plants to improve the instantaneous power output,” IEEE Trans. Energy Conversion, vol. 26, no. 4, pp. 1021-1032, Dec. 2019.

[28] A. J. Garrido, I. Garrido, M. Amundarain, M. Alberdi, and M. D. la Sen, “Sliding-mode control of wave power generation plants,” IEEE Trans. Industry Applications, vol. 48, no. 6, pp. 2372-2381, Nov./Dec. 2018.

[29] G. Bacelli, P. Balitsky, and J. V. Ringwood, “Coordinated control of arrays of wave energy devices–Benefits over independent control,” IEEE Trans. Sustainable Energy, vol. 4, no. 4, pp. 1091-1099, Oct. 2013.

[30] M. I. Marei, M. Mokhtar, and A. A. El-Sattar, “MPPT strategy based on speed control for AWS-based wave energy conversion system,” Renewable Energy, vol. 83, pp. 305-317, Nov. 2015.

[31] S.-Y. Lu, L. Wang, T.-M. Lo, and A. V. Prokhorov, “Integration of wind power and wave power generation systems using a dc microgrid,” IEEE Trans. Industry Applications, vol. 51, no. 4, pp. 2753-2761, Jul./Aug. 2017.

[32] T. Ahmed, “Electrical technologies for grid integration of ocean wave power into the UK national grid,” J. Power Electronics, vol. 10, no. 3, pp. 320-327, May 2018.

[33] N. H. Samrat, N. B. Ahmad, I. A. Choudhury, and Z. B. Taha, “Modeling, control, and simulation of battery storage photovoltaic-wave energy hybrid renewable power generation systems for island electrification in Malaysia,” The Scientific World Journal, pp. 1-21, Apr. 2016.

[34] G. Wang, M. Ciobotaru, and V. G. Agelidis, “Power smoothing of large solar PV plant using hybrid energy storage,” IEEE Trans. Sustainable Energy, vol. 5, no. 3, pp. 834-842, Jul. 2016.

[35] Z. Nie, X. Xiao, Q. Kang, R. Aggarwal, H. Zhang, and W. Yuan, "SMES-battery energy storage system for conditioning outputs from1949-3029 (c) 2016 IEEE